Krahl, Fabian; Giri, Ashutosh; Tomko, John A.; Tynell, Tommi; Hopkins, Patrick E.; Karppinen, Maarit

Thermal Conductivity Reduction at Inorganic-Organic Interfaces

Published in:
Advanced Materials Interfaces

DOI:
10.1002/admi.201701692

Published: 01/06/2018

Document Version
Peer reviewed version

Please cite the original version:
Krahl, F., Giri, A., Tomko, J. A., Tynell, T., Hopkins, P. E., & Karppinen, M. (2018). Thermal Conductivity Reduction at Inorganic-Organic Interfaces: From Regular Superlattices to Irregular Gradient Layer Sequences. Advanced Materials Interfaces, 5(11), [1701692]. https://doi.org/10.1002/admi.201701692

WILEY-VCH

DOI: 10.1002/ ((please add manuscript number))
Article type: Full Paper

Thermal conductivity reduction at inorganic-organic interfaces: From regular superlattices to irregular gradient layer sequences

Fabian Krahl, Ashutosh Giri, John A. Tomko, Tommi Tynell, Patrick E. Hopkins, Maarit Karppinen*

Fabian Krahl,[1] Ashutosh Giri,[2] John A. Tomko,[2] Dr. Tommi Tynell,[1] Prof. Patrick E. Hopkins,[2,3,4] Prof. Maarit Karppinen[1]

[1]Aalto University, Department of Chemistry and Materials Science, Fi-00076 Aalto, Finland
[2]University of Virginia, Department of Mechanical and Aerospace Engineering, Charlottesville, VA 22904, USA
[3]University of Virginia, Department of Materials Science and Engineering, Charlottesville, VA 22904, USA
[4]University of Virginia, Department of Physics, Charlottesville, VA 22904, USA

*corresponding author: maarit.karppinen@aalto.fi

Keywords: thermal conductivity, inorganic-organic interphases, ALD/MLD, thin-film superlattice, gradient material

ABSTRACT: Nanoscale superlattice structures are known to significantly suppress the thermal conductivity in thin films due to phonon scattering at the interfaces of the mutually different layers. Here it is demonstrated that in addition to the number of interfaces, their spacing within the film can lead to a reduction in thermal conductivity. Our proof-of-concept data are for ZnO/benzene thin films fabricated through sequential gas-surface reactions in atomic/molecular layer precision using the atomic/molecular layer deposition (ALD/MLD) technique. In comparison to similarly constructed regular superlattice thin films, thermal conductivity values that are of the same magnitude, or even lower, are achieved for hybrid ZnO/benzene thin films in which the inorganic and organic layers are arranged in a more irregular manner to form various gradient patterns.

1. Introduction

Precise control of thermal conductivity over a wide range of values has been a current challenge in materials science. In particular, the possibility to reduce the thermal conductivity to ultralow levels, on the order of the minimum limit achieved by amorphous phases, are important goals for several applications, including barrier coatings and thermoelectrics.[1–3] Promising advances in this reduction of the thermal conductivity have been made by introducing disorder in the systems via alloying, complex crystal-engineering,[4,5] and by creating interfaces in thin films.[2]

Hicks and Dresselhaus originally proposed that quantum well structures should be capable of lowering the thermal conductivity with only a minor impact on the electrical conductivity;[6] note that the latter point is particularly important for the application in thermoelectrics. Experimentally the phenomenon has been demonstrated e.g. by Hicks et al.[7] in the PbTe/(Pb,Eu)Te system and by Ohta et al.[8] in the $SrTiO_3/Sr(Ti,Nb)O_3$ system. Layered structures that show reduced thermal conductivity have been reported for a number of other material systems as well, such as $CaTiO_3/SrTiO_3$,[9] W/Al_2O_3,[10] PbTe/PbSe,[11] $IrSb_3/CoSb_3$,[12] AlN/GaN,[13] TiNiSn/HfNiSn,[14] Si/Ge (including alloy variants),[15–19] GaAs/AlAs (including alloy variants),[20–23] Bi_2Te_3/Sb_2Te_3,[24] InAs/AlSb,[25] InGaAs/InGaAsP,[26] and Ge_2Te_3/Sb_2Te_3,[27] to name a few. Most such inorganic-inorganic interfaces utilize isoelectronic substitution to retain the electrical conductivity and the high degree of crystallinity of the samples, which essentially grow epitaxially. An exception are the crystalline-amorphous interfaces as reported e.g. in the Al_2O_3/TiO_2 [28] and Si [29] systems.

With regard to high-quality interfaces, inorganic-organic superlattices offer an attractive option to reduce thermal conductivity compared to a homogeneous inorganic thin film. Owing to the large acoustic impedances between the inorganic and organic materials, we may anticipate considerably lowered thermal boundary conductance across the inorganic-organic interface.[30] Remarkable results have been reported for e.g. TiS_2 with organic molecules

intercalated either electrochemically[31] or chemically[32] from an organic solution. We have, on the other hand, fabricated ZnO/benzene [33,34] and TiO_2/benzene[35,36] superlattices using the gas-phase atomic/molecular layer deposition (ALD/MLD) thin-film technique to demonstrate reductions in thermal conductivity of several orders of magnitude. Among the benefits of the ALD/MLD technique over solution-based intercalation routes is that it allows the precise control of the introduction frequency of the organic layers within the inorganic matrix.

The uniting concept to lower the thermal conductivity of superlattice and nanolaminate structures is to suppress phonon transmission across the thin film by reducing the phonon mean free path, l_{mfp}, through incoherent scattering at the superlattice interfaces achieved via precise control over the period thicknesses. In the kinetic theory description, l_{mfp} is related to the thermal conductivity, $\kappa_{phon.}$, by the relation, $\kappa_{phon} \equiv 1/3\ C\nu\ l_{mfp}$, where C is the heat capacity per unit volume and v the average phonon velocity.[37] Therefore, in the incoherent phonon scattering regime, the introduction of interfaces with period thicknesses smaller than l_{mfp} is an effective way to reduce thermal conductivity in superlattices and nanolaminates. In this regard, the smaller the separation between interfaces in the superlattice structures, the more pronounced the reduction in thermal conductivity for these structures. However, having fewer interfaces in the material could be advantageous from an overall performance or material fabrication perspective.

In the present work, we investigate the impact of regular versus irregular/disordered layer arrangements in inorganic-organic hybrid thin films taking the advantage of the ALD/MLD technique for layer engineering. The ALD/MLD technique is uniquely suited for engineering these types of carefully designed structures, because its self-limiting gas-surface reactions enable atomic/molecular level film growth control.[38–40] We chose the ZnO/benzene system as our model system because (i) in ZnO heat conduction is dominated by phonons rather than by charge carriers,[41] (ii) the ALD/MLD process for ZnO/benzene thin films is already established

allowing the fabrication of the films in a highly controlled manner,[34,42–44] and (iii) in these superlattices the phonon mean free path is of the relevant length.[33,45] We then compare ZnO/benzene thin films of regular superlattice structure (where the ZnO/benzene period thicknesses are uniform throughout the thin film) with hybrid films where we have an increasing (or decreasing) gradient for the ZnO layer spacing between consequent organic layers. Our work reveals that – in comparison to superlattice thin films with regularly spaced period thicknesses – the same, or even lower thermal conductivity values can be achieved for our hybrid ZnO/benzene thin films where the inorganic and organic layers are arranged in an irregular manner.

2. Results and Discussion

Altogether twelve ZnO/benzene thin-film samples with a varying total number and frequency of the benzene barrier layers were investigated. For all these samples, the total number of ALD (for ZnO) plus MLD (for benzene) cycles was fixed to 613±8 such that the resultant overall film thickness was of the order of 100 nm. The total number of MLD cycles applied varied from 5 to 25. In most of the samples each barrier layer consisted of a single benzene ring layer. However, for two "special" samples thicker (ZnO-benzene) hybrid barrier blocks were deposited. Sketches of the resultant thin-film structures are shown in **Figure 1**, while **Table 1** summarizes the sample naming scheme, the sequence of the ALD/MLD cycles applied for the sample fabrication, the resultant individual layer thicknesses and the total film thicknesses for the samples studied. The superlattice (regularly spaced) samples are denoted SL and the gradient-material (irregular spacing) samples GM. In both cases the name, SL or GM, is followed by the number of barrier layers (and their thickness in parentheses), then by the gradient, and finally – if necessary – by another distinctive feature. For example, GM-12(1)/±8-M is a gradient material with 12 barrier layers; each barrier layer consists of a single benzene

layer (made by applying one MLD cycle), a gradient of ±8 and a mirror plane in the middle of the film (cf. Figure 1). Seen from Table 1 is that this GM-12(1)/±8-M sample was deposited by applying 69, followed by 61, then 53 and so on ALD cycles (reducing the number of cycles by 8 each time) until the middle layer only consisted of 21 ALD cycles, afterwards the number of ALD cycles was increased six times by 8 for each ZnO layer until the final layer again was deposited with 69 ALD cycles. In this GM-12(1)/±8-M sample all the ZnO layer are separated by a single MLD cycle (indicated by "/" in Table 1) to deposit the benzene barrier layers, each of ~0.4 nm in thickness. The result is a gradient-material structure where the ZnO-layer thickness is decreasing by ~1.1 nm from substrate to the middle of the film and then again starts increasing from the middle of the film towards the top in the same manner.

To illustrate the quality of our ZnO/benzene hybrid thin films, we display in **Figure 2** XRR and GIXRD patterns for a representative SL and several GM samples. The XRR data confirm that our films are in the target thickness range of ca. 100 nm. We also determined the surface/interface roughness values for the SL samples from the XRR data; the roughness was estimated to be in the order of few nanometers. From Figure 2 also seen is that – as expected – the symmetry seen in the XRR patterns of the pure ZnO and the ZnO/benzene SL films breaks down as soon as a gradient is introduced. The GIXRD data confirm that all the samples are crystalline; all the diffraction peaks seen are of the polycrystalline ZnO wurtzite structure. The GIXRD patterns in Figure 2 show the three most pronounced peaks of ZnO; it can be seen that the reflection from the c-plane (002) decreases for the hybrids compared to plain ZnO while the a-plane (100) reflection gains intensity. Not surprisingly the crystallinity seems to decrease slowly with increasing frequency of the organic layers (compare e.g. GM-12(1)/±8-M-2 to SL-5(1)). However, between the SL and GM films of the same total number of organic layers no notable difference in crystallinity is observed (compare e.g. SL-5(1) and GM-5(1)/-20 in Figure 2).

The mean free path for phonons (l_{mfp}) in our material was calculated by the gray-medium approximation using the kinetic theory to be ~13.2 nm and therefore being in the range or above our ZnO-block thicknesses (see experimental section for more details). The measured cross-plane thermal conductivity values are listed in Table 1 and for the superlattice structures (including previously reported ones[33,34]) and linear gradients also plotted in **Figure 3** against the average ZnO layer thickness. This thickness is of course directly proportional to the number of ALD cycles used for each layer. **Figure 4** shows the thermal conductivities of all investigated samples and previously reported superlattices[33,34] against the number of benzene separation layers. As a general observation from Figure 4, nearly all films follow the trend of more benzene barrier layers leading to a lower thermal conductivity, though also among the films with the same number of benzene layers the thermal conductivity varies, depending on the layer-sequence design.

We first discuss the thermal conductivity of our linear-gradient films, GM-5(1)/+20, GM-5(1)/+20-2, GM-5(1)/-20, and GM-12(1)/+7. The first three of these films have the same number of barrier layers; the only difference is in the sequence of the layers (see Table 1 and Figure 1). The GM-5(1)/+20 film is essentially similar to GM-5(1)/-20 but flipped such that in GM-5(1)/+20 the benzene barrier layers are packed tighter at the bottom (at the substrate) while in GM-5(1)/-20 the barrier layers are packed tighter at the top. The GM-5(1)/+20-2 sample is a repetition of GM-5(1)/+20 to ensure repeatability. Within experimental uncertainties, all these three films have similar thermal conductivities between 8.1 and 9.3 W m^{-1} K^{-1}. This indicates that the direction of the gradient within the film is not an important factor controlling the thermal conductivity, an assumption that is strengthened further by GM-5(1)/20-S, a sample that has the same ZnO layer thicknesses as e.g. GM-5(1)/+20 but in a shuffled order; this film too has a similar thermal conductivity within the experimental uncertainty. On the other hand, the periodic superlattice SL-5(1) with the same number of benzene barrier layers has a thermal conductivity of 11.8 W m^{-1} K^{-1} that is higher than those of the corresponding gradient materials.

Therefore, it is safe to claim that the gradient materials may be at least as efficient in suppressing the thermal conductivity as the superlattices, and through judicious GM design even considerably lower thermal conductivity values may be realized for the gradient materials such as the up to ~31% lower values seen here for the SL-5(1) structure.

In the case of 12 benzene barrier layers the beneficial effect of the irregular arrangement of the barrier layers is not seen though, as the GM-12(1)/+7 film has a thermal conductivity of 4.6 ± 0.5 W m^{-1} K^{-1} (Table 1) which is similar to but not lower than our previously reported (κ = 4.2 ± 0.5 W m^{-1} K^{-1})[34] and current (κ = 3.9 ± 0.4 W m^{-1} K^{-1}) values for the superlattice SL-12(1). With 12 barrier layers the linear gradient of sample GM-12(1)/+7 cannot be very steep when the overall film thickness is 100 nm, so instead of the difference of 20 cycles between layers (e.g. in GM-5(1)/+20 and GM-5(1)/-20) the difference is only 7 cycles in GM-12(1)/+7 which may not be enough to induce a significant suppression in thermal conductivity.

Next, we turn our attention to the nonlinear GM thin films, GM-12(1)/Fib, GM-12(1)/±8-M and GM-12(1)/±8-M-rev. Of these samples, GM-12(1)/Fib has a very steep nonlinear gradient following the Fibonacci series (see Table 1), however, its thermal conductivity is significantly higher compared to the corresponding SL or other gradient films. This could be due to the steep gradient in the film as the last ZnO layer thickness is a third of the films total thickness; thus, it might be more accurate to view the film as a combination of a steep gradient film topped by a separate 223-cycle (~35 nm) thick ZnO film. The two films, GM-12(1)/±8-M and GM-12(1)/±8-M-rev, both have a mirror plane parallel to the layers, so one could view them as two 50-nm gradient films stacked on top of each other, resulting in an overall slightly smaller thermal conductivity compared to their SL counterpart. As the error margins overlap with the corresponding superlattice (SL-12(1)), we can only state that their thermal conductivity is at least as low as that of the corresponding SL-12(1) film.

We also fabricated GM thin films with thicker hybrid barrier layers, where the barrier layer is not a single-benzene-molecule thick but consists of a stack of benzene layers linked by Zn-

O bridges. GM-5(5)/-20 is a linear gradient otherwise similar to GM 5(1)/-20, but the barrier layers consist of 5 HQ-DEZ cycles each instead of only 1 cycle. The effect is a drastic reduction in thermal conductivity compared to the GM-5(1)/-20 sample. This clearly demonstrates that the barrier layer thickness plays a significant role in dictating thermal conductivity. We may also compare GM-5(5)/-20 with our previously reported superlattice SL-24(1)[33] with nearly the same total number of HQ-DEZ cycles but scattered homogeneously; it is seen from Figure 4 that among the two samples, GM-5(5)/-20 and SL-24(1), thermal conductivity is considerably lower for the latter. Thus, to minimize the thermal conductivity it is beneficial to scatter the benzene layers instead of bundling them together. This is further supported by our results for the sandwich sample, which has 12 Zn-O-benzene layers bunched together in the middle of the sample instead of evenly spreading these layers; from Table 1, thermal conductivity is 8.9 $Wm^{-1}K^{-1}$ for GM-12(1)/+7, while being 3.9 $Wm^{-1}K^{-1}$ for SL-12(1).

Finally, we discuss the reasons for the consistently lower thermal conductivity in the gradient material samples. The most straightforward and simple explanation is based on the crystallinity of the samples. As the ZnO blocks between the benzene layers get thinner and thinner their crystallinity tends to decrease until they become amorphous (as previously reported by us[33]), so it seems reasonable that, while all layers in the superlattice are crystalline, the thinner ZnO layers in the gradient material could be partially amorphous and thus we would not only introduce a benzene boundary, but also reduce the crystallinity, which concomitantly lowers the thermal conductivity of the thin film. However, evidence of crystallinity and disorder in individual layers can not be inferred from the GIXRD results; the GIXRD patterns indicate crystalline films, but they provide an average of the whole film and the very thin, amorphous layer (if present) may not have a detectable influence on the pattern since the vast majority of the sample is still crystalline. Also, this explanation based on disordered layers for the thinnest layers alone can not explain the results for GM-12(1)/+7 and GM-12(1)/Fib, which, despite having thinner ZnO layers, have a higher thermal conductivity than the superlattice SL-12(1).

Another possible reason for the observed lower thermal conductivity in the gradient materials could arise from the fact that superlattices – in accord with the phonon filter described by Narayanamurti et al.[20] – selectively suppress phonons with wavelengths similar to 2d with d being the superlattice period, while offering maximum transmission for phonons with wavelengths comparable to d;[46] this would follow provided that the system behaves as an optical system with the acoustic impedance of the different layers being for phonons what the refractive index is for photons in an optical system. Some of our gradient materials would then be reminiscent of chirped mirrors consisting of discrete layers in photonics that are used to reflect not only a specific wavelength but a range of wavelengths for e.g. broadband reflection, see e.g. ref. 47. From this perspective, we believe that there is a strong possibility that gradient materials indeed can have a better overall suppression of different phonon wavelengths by introducing disorder, which would explain the lower thermal conductivity in some gradient materials compared to superlattices. If this were the case, introducing a gradient would be a general way to reduce thermal conductivity that would be viable also in pure inorganic systems where crystallinity is not degraded from smaller superlattice periods.

3. Conclusions

We have demonstrated the significance of the spacing of barrier layers for the suppression of thermal conductivity in regular inorganic-organic superlattice thin films and in otherwise similar thin films but with an irregular spacing of the inorganic-organic interfaces. In the hybrid thin-film structures investigated, ALD-grown ZnO layers alternate with monomolecular MLD-grown benzene layers. For all the hybrid thin films thermal conductivity is considerably lowered compared to pure ZnO.

Most excitingly, the way the benzene barrier layers were positioned within the thin-film structure was found to have a measurable effect on the thermal conductivity of the film.

Comparison of films with the benzene layers either bunched together or spread out in a regular or irregular fashion revealed that the most pronounced suppression of thermal conductivity for a given number of benzene layers could be achieved by a gradient structure where the separation between subsequent benzene layers was varied. This was tentatively attributed to either an aselective suppression of different phonon wavelengths or a possible subtle reduction of the crystallinity of the film. To truly engineer the minimum thermal conductivity with a set number of barrier layers would require deep understanding of phonon transport across these barriers, but we hope that our work is a step ahead towards this goal, as to our knowledge these results are the first reported thermal conductivity measurements of thin films with engineered layer-gradient structures.

We positively believe that the benefits of disorder in a gradient structure compared to an ordered superlattice structure is not limited to the present ZnO-benzene system but could be extended to other two-component layer-stacking systems as well. Moreover, the same concept could possibly be transferred to the design of acoustic chirped mirrors, though this was not attempted in the present work. It is important to note that the combined ALD/MLD technique is a simple but elegantly suited approach for the fabrication of various imaginable – regular or irregular – layer-sequence patterns, as was well shown in the present work already. This is remarkable, as complex interface design has become a major issue in nanoscience and – technolgy to create and control various material properties, e.g. polarization, magnetization, superconductivity, and more.[48-50]

4. Experimental Section

All the thin film samples were deposited in a Picosun R-100 ALD reactor using diethyl zinc (DEZ; >52 w% Zn basis from Sigma-Aldrich), deionised water and hydroquinone (HQ; ≥99.5% Reagent Plus from Sigma-Aldrich) as precursors. In each deposition experiment thin films were

simultaneously grown in the reactor at the same time on a 1x1 cm sapphire substrate (from MTI, cut parallel to (001) plane) for the thermal conductivity measurements and a ca. 3x3 cm silicon substrate (from Okmetic, cut parallel to the (100) plane, p-type) for the thickness measurements. The substrate temperature was set at 230 °C. During the depositions, the DEZ and water sources were kept at room temperature, while the HQ source was held at 150 °C to ensure a high enough vapour pressure. Pulse/purge times were 0.3 s/4 s for DEZ, 0.5 s/4 s for water and 15 s/30 s for HQ, purging was done with nitrogen (99.999% purity), generated by a Parker nitrogen generator (model: HPN2-5000C-L-230V). The precursor pulse and N_2 purge times differ from our previous works[33,34,43] due to using the R-100 reactor instead of the F-120 reactor used in the previous reports. With these deposition parameters the growth-per-cycle (GPC) was determined (from the film thickness data) to be 1.8 Å/cycle for the DEZ/H_2O ALD cycles and ca. 4.0 Å/cycle for DEZ/HQ MLD cycles; these values are in line with previously reported growth rates for ZnO and ZnO-benzene thin films.[43,51,52]

The film thicknesses were determined for the regular superlattice thin films based on X-ray reflectivity (XRR; Panalytical X'Pert Pro machine using Cu Kα radiation generated with 40 kV and 45 mA) measurements. The XRR method uses the position and width of so-called Kiessig fringes to determine the film thickness (see Figure 2). In the case of homogeneous single-material thin films such as our pure ZnO films these fringes are regularly spaced and the thickness determination is straightforward. For the regular ZnO-benzene SL thin films a periodic occurrence of higher peaks is seen, corresponding to reflections from the organic layers, confirming the presence of a superlattice and allowing the determination of the SL periodicity. For the gradient materials a multitude of different sized peaks are seen, and the thickness determination is therefore more prone to small uncertainties. Nevertheless, the total film thickness and the individual layer thicknesses could be well estimated for the gradient films, the latter based on the GPC values determined for the DEZ/H_2O ALD and the DEZ/HQ MLD cycles in the case of pure ZnO and ZnO-benzene SL films. By simulating SL-5(1) and matching

the simulation to the measurement data with the X'Pert Reflectivity program v1.3 from PANalytical an estimate of the roughness (3 nm) could be made. For the irregular samples such simulations could not reasonably be made as we get too many variables, but as these films are grown under the same conditions we find it safe to assume that the roughness will not differ greatly. Crystallinity of the films was evaluated with grazing incidence X-ray diffraction (GIXRD) measurements using the same diffractometer with the angle of the incoming beam being held constantly at 0.5°. All X-ray measurements were made on samples deposited on silicon substrates.

The time-domain thermoreflectance (TDTR) technique was used for the thermal conductivity measurements. It is a non-contact, optical pump-probe technique used to measure the thermal properties of materials by relating the change in reflectance of the sample surface (that is related to the temperature change) to the thermal properties of the sample of interest.[53–55] The specific details of our experimental setup and the analysis procedure to measure the thermal conductivity of our hybrid thin films are given in Refs. 33 and 36.

We calculated an average phonon mean free path for ZnO under the gray-medium approximation using the kinetic theory expression, $\kappa = 1/3\ C_V l_{mfp}$.[56] The group velocities for the transverse and longitudinal acoustic modes (under the Debye approximation) were calculated using the phonon dispersion in the $\Gamma \rightarrow M$ as given in Ref. 57; 2281 and 5662 ms^{-1} were used for transverse and longitudinal group velocities, respectively, and the experimentally determined heat capacity of ZnO was taken from Ref. 58 (C_V =2.8 J cm^{-3} K^{-1}) to determine a phonon mean free path of ~13.2 nm under the gray-medium approximation. Since most of the ZnO layer thicknesses in our study are less than or comparable to this length scale, the thermal conductivity for our structures can be greatly reduced by introducing interfaces between the inorganic layers. This is in line with our results from Ref. 33 for regularly spaced ZnO/HQ SLs, where we show that for ZnO layer thicknesses in the range of 0.7 to 13.1 nm, phonon transport

in the inorganic layer is ballistic and that the phonons scatter only at boundaries that restore local thermodynamic equilibrium.[4] In other words, the phonon mean free path for the SL structures is limited by the ZnO layer thicknesses. Furthermore, it is well known that this gray-medium approximation for the mean free path can greatly under predict the majority of the spectral mean free paths in crystalline solids, thus, our calculation is a conservative estimate for the phonon mean free paths in the ZnO layer. For example, first principles calculations from Wu et al.[59] demonstrate that ~60% of the contribution to the total thermal conductivity comes from phonons with mean free paths greater than 50 nm, which is larger than the ZnO layer thicknesses used in this study, further supporting our assertion that the ZnO layer thicknesses limit the phonon mean free paths in our systems.

Acknowledgements

The present work has received funding from the European Research Council under the European Union's Seventh Framework Programme (FP/2007-2013)/ERC Advanced Grant Agreement (No. 339478) and Academy of Finland (No. 296299), and also from Aalto University through the graduate student grant of School of Chemical Engineering. PEH and AG appreciate support from the United States Army Research Office, Grant Number W911NF-16-1-0320.

Received: ((will be filled in by the editorial staff))
Revised: ((will be filled in by the editorial staff))
Published online: ((will be filled in by the editorial staff))

[1] G. Pernot, M. Stoffel, I. Savic, F. Pezzoli, P. Chen, G. Savelli, A. Jacquot, J. Schumann, U. Denker, I. Mönch, C. Deneke, O. G. Schmidt, J. M. Rampnoux, S. Wang, M. Plissonnier, A. Rastelli, S. Dilhaire, N. Mingo, *Nat. Mater.* **2010**, *9*, 491.
[2] G. J. Snyder, E. S. Toberer, *Nat. Mater.* **2008**, *7*, 105.
[3] P. M. Norris, N. Q. Le, C. H. Baker, *J. Heat Transfer* **2013**, *135*, 061604.
[4] G. S. Nolas, J. Poon, M. Kanatzidis, *MRS Bull.* **2006**, *31*, 199.
[5] K. Koumoto, I. Terasaki, R. Funahashi, *MRS Bull.* **2006**, *31*, 206.
[6] L. D. Hicks, M. S. Dresselhaus, *Phys. Rev. B* **1993**, *47*, 12727.

[7] L. D. Hicks, T. C. Harman, X. Sun, M. S. Dresselhaus, *Phys. Rev. B* **1996**, *53*, R10493.
[8] H. Ohta, S. Kim, Y. Mune, T. Mizoguchi, K. Nomura, S. Ohta, T. Nomura, Y. Nakanishi, Y. Ikuhara, M. Hirano, H. Hosono, K. Koumoto, *Nat. Mater.* **2007**, *6*, 129.
[9] J. Ravichandran, A. K. Yadav, R. Cheaito, P. B. Rossen, A. Soukiassian, S. J. Suresha, J. C. Duda, B. M. Foley, C.-H. Lee, Y. Zhu, A. W. Lichtenberger, J. E. Moore, D. A. Muller, D. G. Schlom, P. E. Hopkins, A. Majumdar, R. Ramesh, M. A. Zurbuchen, *Nat. Mater.* **2014**, *13*, 168.
[10] R. M. Costescu, D. G. Cahill, F. H. Fabreguette, Z. A. Sechrist, S. M. George, *Science* **2004**, *303*, 989.
[11] D. G. Cahill, A. Bullen, S.-M. Lee, in *High Temperatures - High Pressures*, **2000**, p. 135–142 (159–166 in 15th ECTP Proceedings).
[12] D. W. Song, W. L. Liu, T. Zeng, T. Borca-Tasciuc, G. Chen, J. C. Caylor, T. D. Sands, *Appl. Phys. Lett.* **2000**, *77*, 3854.
[13] Y. K. Koh, Y. Cao, D. G. Cahill, D. Jena, *Adv. Funct. Mater.* **2009**, *19*, 610.
[14] P. Hołuj, C. Euler, B. Balke, U. Kolb, G. Fiedler, M. M. Müller, T. Jaeger, E. Chávez Angel, P. Kratzer, G. Jakob, *Phys. Rev. B* **2015**, *92*, 125436.
[15] T. Koga, S. B. Cronin, M. S. Dresselhaus, J. L. Liu, K. L. Wang, *Appl. Phys. Lett.* **2000**, *77*, 1490.
[16] S. T. Huxtable, A. R. Abramson, C.-L. Tien, A. Majumdar, C. LaBounty, X. Fan, G. Zeng, J. E. Bowers, A. Shakouri, E. T. Croke, *Appl. Phys. Lett.* **2002**, *80*, 1737.
[17] T. Borca-Tasciuc, W. Liu, J. Liu, T. Zeng, D. W. Song, C. D. Moore, G. Chen, K. L. Wang, M. S. Goorsky, T. Radetic, R. Gronsky, T. Koga, M. S. Dresselhaus, *Superlatt. Microstruct.* **2000**, *28*, 199.
[18] S.-M. Lee, D. G. Cahill, R. Venkatasubramanian, *Appl. Phys. Lett.* **1997**, *70*, 2957.
[19] S. Chakraborty, C. A. Kleint, A. Heinrich, C. M. Schneider, J. Schumann, M. Falke, S. Teichert, *Appl. Phys. Lett.* **2003**, *83*, 4184.
[20] V. Narayanamurti, H. L. Störmer, M. A. Chin, A. C. Gossard, W. Wiegmann, *Phys. Rev. Lett.* **1979**, *43*, 2012.
[21] W. S. Capinski, H. J. Maris, T. Ruf, M. Cardona, K. Ploog, D. S. Katzer, *Phys. Rev. B* **1999**, *59*, 8105.
[22] M. N. Luckyanova, J. Garg, K. Esfarjani, A. Jandl, M. T. Bulsara, A. J. Schmidt, A. J. Minnich, S. Chen, M. S. Dresselhaus, Z. Ren, E. A. Fitzgerald, G. Chen, *Science* **2012**, *338*, 936.
[23] M. N. Luckyanova, J. A. Johnson, A. A. Maznev, J. Garg, A. Jandl, M. T. Bulsara, E. A. Fitzgerald, K. A. Nelson, G. Chen, *Nano Lett.* **2013**, *13*, 3973.
[24] R. Venkatasubramanian, *Phys. Rev. B* **2000**, *61*, 3091.
[25] S. S. P. T. Borca-Tasciuc D. Achimov, W. L. Liu, G. Chen, H. W. Ren, C. H. Lin, *Microsc. Therm. Eng.* **2001**, *5*, 225.
[26] Y. Zhang, Y. Chen, C. Gong, J. Yang, R. Qian, Y. Wang, *J. Microelectromech. Syst.* **2007**, *16*, 1113.
[27] H. Tong, X. S. Miao, X. M. Cheng, H. Wang, L. Zhang, J. J. Sun, F. Tong, J. H. Wang, *Appl. Phys. Lett.* **2011**, *98*, 101904.
[28] S. Ali, T. Juntunen, S. Sintonen, O. M. E. Ylivaara, R. L. Puurunen, H. Lipsanen, I. Tittonen, S.-P. Hannula, *Nanotechnol.* **2016**, *27*, 445704.
[29] A. France-Lanord, S. Merabia, T. Albaret, D. Lacroix, K. Termentzidis, *J. Phys. Condens. Matter* **2014**, *26*, 355801.
[30] J.-P. Niemelä, A. J. Karttunen, M. Karppinen, *J. Mater. Chem. C* **2015**, *3*, 10349.
[31] C. Wan, X. Gu, F. Dang, T. Itoh, Y. Wang, H. Sasaki, M. Kondo, K. Koga, K. Yabuki, G. J. Snyder, R. Yang, K. Koumoto, *Nat. Mater.* **2015**, *14*, 622.
[32] R. Tian, C. Wan, Y. Wang, Q. Wei, T. Ishida, A. Yamamoto, A. Tsuruta, W. Shin, S. Li, K. Koumoto, *J. Mater. Chem. A* **2017**, *5*, 564.

[33] A. Giri, J.-P. Niemelä, T. Tynell, J. T. Gaskins, B. F. Donovan, M. Karppinen, P. E. Hopkins, *Phys. Rev. B* **2016**, *93*, 115310.
[34] T. Tynell, A. Giri, J. Gaskins, P. E. Hopkins, P. Mele, K. Miyazaki, M. Karppinen, *J. Mater. Chem. A* **2014**, *2*, 12150.
[35] J.-P. Niemelä, A. Giri, P. E. Hopkins, M. Karppinen, *J. Mater. Chem. A* **2015**, *3*, 11527.
[36] A. Giri, J.-P. Niemelä, C. J. Szwejkowski, M. Karppinen, P. E. Hopkins, *Phys. Rev. B* **2016**, *93*, 024201.
[37] C. Kittel, *Introduction to Solid State Physics*, John Wiley & Sons, Inc., **2005**.
[38] O. Nilsen, K. Klepper, H. Nielsen, H. Fjellvåg, *ECS Transactions* **2008**, *16*, 3.
[39] S. M. George, B. Yoon, A. A. Dameron, *Acc. Chem. Res.* **2009**, *42*, 498.
[40] P. Sundberg, M. Karppinen, *Beilstein J. Nanotechnol.* **2014**, *5*, 1104.
[41] Ü. Özgür, Y. I. Alivov, C. Liu, A. Teke, M. A. Reshchikov, S. Doğan, V. Avrutin, S.-J. Cho, H. Morkoç, *J. Appl. Phys.* **2005**, *98*, 041301.
[42] T. Tynell, I. Terasaki, H. Yamauchi, M. Karppinen, *J. Mater. Chem. A* **2013**, *1*, 13619.
[43] T. Tynell, M. Karppinen, *Thin Solid Films* **2014**, *551*, 23.
[44] B. Yoon, B. H. Lee, S. M. George, *J. Phys. Chem. C* **2012**, *116*, 24784.
[45] A.J. Karttunen, T. Tynell, M. Karppinen, *Nano Energy* **2016**, *22*, 338.
[46] M. J. Kelly, *J. Phys. C* **1985**, *18*, 5963.
[47] R. Paschotta, *Encyclopedia of Laser Physics and Technology*, Wiley VCH, **2008**.
[48] H. Y. Hwang, Y. Iwasa, M. Kawasaki, B. Keimer, N. Nagaosa, Y. Tokura, *Nat. Mater.* **2012**, *11*, 103.
[49] A. J. Grutter, A. Vailionis, J. A. Borchers, B. J. Kirby, C. L. Flint, C. He, E. Arenholz, Y. Suzuki, *Nano Lett.* **2016**, *16*, 5647.
[50] G. De Luca, N. Strkalj, S. Manz, C. Bouillet, M. Fiebig, M. Trassin, *Nat. Commun.* **2017**, *8*, 1419.
[51] T. Tynell, M. Karppinen, *Semicond. Sci. Technol.* **2014**, *29*, 043001.
[52] B. Yoon, Y. Lee, A. Derk, C. Musgrave, S. George, *ECS Transactions* **2011**, *33*, 191.
[53] C. A. Paddock, G. L. Eesley, *J. Appl. Phys.* **1986**, *60*, 285.
[54] P. E. Hopkins, J. R. Serrano, L. M. Phinney, S. P. Kearney, T. W. Grasser, C. T. Harris, *J. Heat Transfer* **2010**, *132*, 081302.
[55] D. G. Cahill, *Rev. Sci. Instrum.* **2004**, *75*, 5119.
[56] G. Chen, *MIT-Pappalardo Series in Mechanical Engineering* Oxford University Press **2005**
[57] J. Serrano, F. Manjón, A. Romero, A. Ivanov, M. Cardona, R. Lauck, A. Bosak, M. Krisch, *Phys. Rev. B* **2010**, *81*, 174304.
[58] C. Klingshirn, A.Waag, A. Hoffmann, and J. Geurts, Zinc Oxide: From Fundamental Properties Towards Novel Applications, Springer Series in Material Science. **2010**, Vol. 120.
[59] X. Wu, J. Lee, V. Varshney, J. L. Wohlwend, A. K. Roy, T. Luo, *Sci. Reports* **2016**, *6*, 22504 EP.
[60] J. Alvarez-Quintana, E. Martínez, E. Pérez-Tijerina, S. A. Pérez-García, J. Rodríguez-Viejo, *J. Appl. Phys.* **2010**, *107*, 063713.

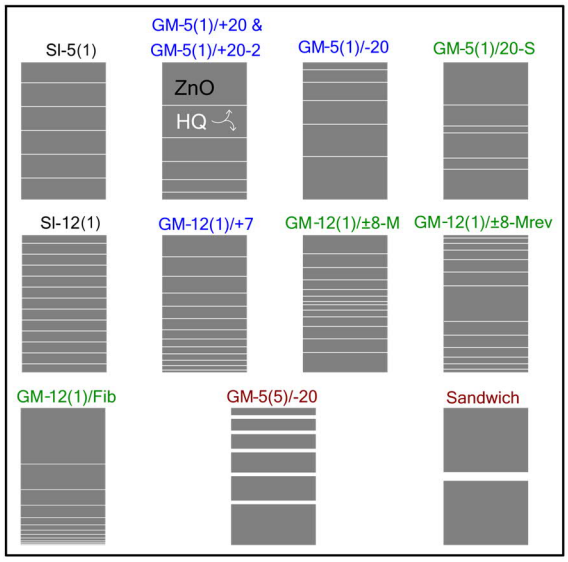

Figure 1. All investigated thin film designs.
Sketch not to scale.

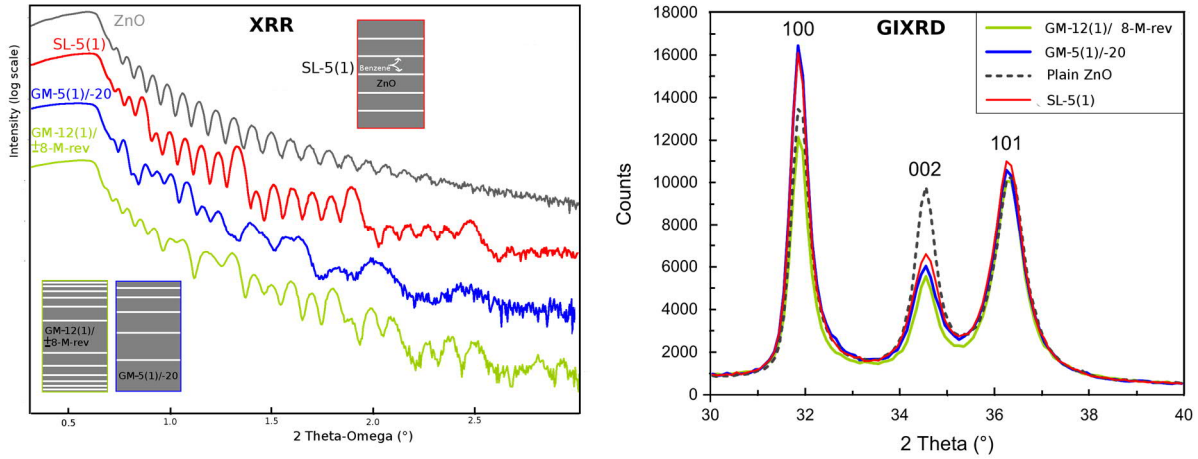

Figure 2. *Left:* XRR curves for ZnO, a superlattice (sample SL-5) and two gradient materials (GM-20/5 & GM±8/12-M-rev), inlets are sketches of the films cross sections (not to scale). *Right:* GIXRD curves for the main peaks of ZnO, same samples as in the XRR on the left.

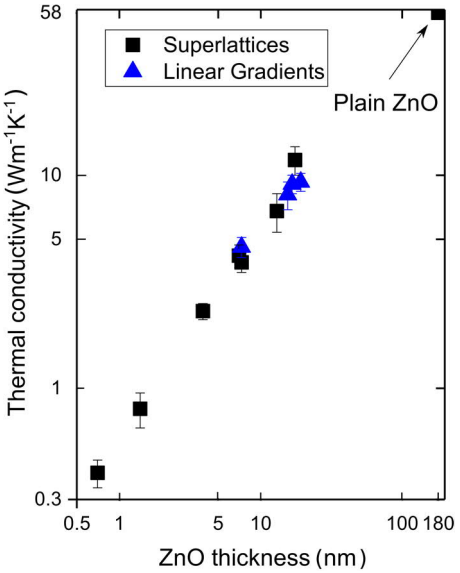

Figure 3: Average ZnO block thickness compared to thermal conductivity of superlattices and linear Gradients, Value for plain ZnO is from Alvarez et al.[60]

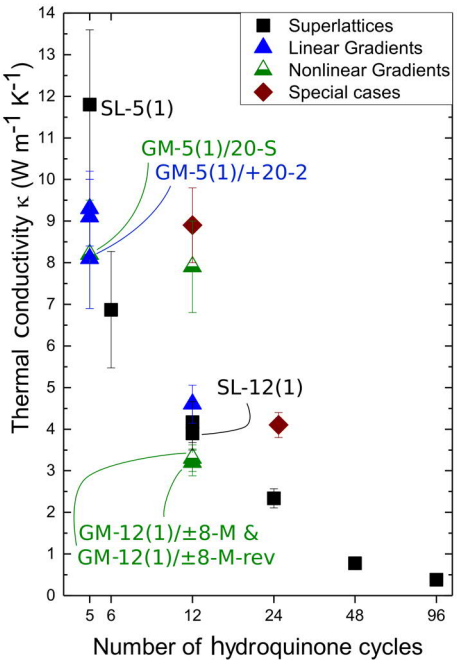

Figure 4. Thermal conductivity plotted against the number of HQ-DEZ cycles. Squares indicate the SLs (unlabelled ones are previously reported[33,34]), triangles gradient materials. The diamond shapes are samples with the HQ-Zn layers not spread out completely. For a more detailed description of samples see Table 1.

Table 1. Naming and structures of the samples investigated and their measured thermal conductivity values. Cycle sequence is listed from substrate to top, "/" represents 1 DEZ-HQ MLD cycle and the number of DEZ-H_2O ALD cycles (e.g. GM-12(1)/+7 starts with 11 and ends with 95 DEZ-H_2O cycles, and has a total of 12 DEZ-HQ cycles distributed in between). For the thickness a constant width of 0.4 nm/cycle for each DEZ-HQ layer was assumed and the ZnO layers were then calculated using that value and the measured overall film thickness.

Sample	cycle sequence	ZnO Layer thickness [nm]	Film Thickness [nm]	κ [W m^{-1} K^{-1}]	Symbol [Figure 4]
Superlattices					
SL-5(1)	5x (100/)+100	5x(17.2/)+17.2	105 ± 5	11.8 ± 1.8	■
SL-12(1)	12x(46/)+46	12x(7/)+7	95 ± 5	3.9 ± 0.4	■
Linear Gradients					
GM-5(1)/-20	150/130/110 /90/70/50	28.1/24.3/20.6/ 16.8/13.1/9.4	115 ± 5	9.3 ± 0.9	▲
GM-5(1)/+20	50/70/90/ 110/130/150	8.2/11.5/14.5/ 17.7/20.9/24.1	100 ± 5	9.1 ± 0.9	▲
GM-5(1)/+20-2	50/70/90/ 110/130/150	7.5/10.4/13.4/ 16.4/19.4/22.4	93 ± 5	8.1 ± 1.2	▲
GM-12(1)/+7	11/18/25/32/ 39/46/53/60/ 67/74/81/ 88/95	1.4/2.4/3.3/4.2/ 5.1/6.0/6.9/7.9/ 8.8/9.7/10.6/ 11.5/12.4	95 ± 5	4.6 ± 0.5	▲
Nonlinear Gradients					
GM-5(1)/20-S	130/70/110/ 50/90/150	18.1/9.8/15.3/ 7.0/12.5/20.9	87 ± 5	8.2 ± 1.3	△
GM-12(1)/Fib	1/1/2/3/5/8/ 13/21/34/55/ 89/144/233	0.1/0.1/0.3/0.4/ 0.7/1.2/1.9/3.1/ 5.0/8.1/13.2/ 21.3/34.5	95 ± 5	7.9 ± 1.1	△
GM-12(1)/±8-M	69/61/53/ 45/37/ 29/21/29/ 37/45/ 53/61/69	9.9/8.7/7.6/ 6.4/5.3/ 4.1/3.0/4.1/ 5.3/6.4/ 7.6/8.7/9.9	92 ± 5	3.2 ± 0.3	△
GM-12(1)/±8-M-rev	24/32/40/ 48/56/ 64/72/64/ 56/48/ 40/32/24	3.5/4.7/5.8/ 7.0/8.1/ 9.3/10.5/9.3/ 8.1/7.0/ 5.8/4.7/3.5	92 ± 5	3.3 ± 0.3	△
Special cases					
GM-5(5)/-20	150/////130///// 110/////90///// 70/////50	28.3/////24.5 /////20.7///// 17.0/////13.2 /////9.4	125 ± 5	4.1 ± 0,3	◆
Sandwich	300//////////300	43.6//////////43.6	92 ± 5	8.9 ± 0,9	◆

Table of contents entry

The present article investigates thermal conductivity of ZnO thin films with ZnO/benzene interfaces. Thin films with disordered internal structure (gradient materials) are compared to thin films with an ordered internal structure (superlattices). The article shows that thin films with an intrinsic disordered gradient structure can be as efficient, or even better, in suppressing the thermal conductivity as their ordered superlattice counterparts.

Keyword: Thermal conductivity

F. Krahl 1, A. Giri 2, J. A. Tomko 2, T. Tynell 1, P. E. Hopkins 2,3,4, M. Karppinen* 1

Thermal conductivity reduction at inorganic-organic interfaces: From regular superlattices to irregular/gradient layer sequences